

Morphology and Surface Area of Emulsion-Derived (PolyHIPE) Solid Foams Prepared with Oil-Phase Soluble Porogenic Solvents: Three-Component Surfactant System

Andrea Barbetta[†] and Neil R. Cameron*

Department of Chemistry, University of Durham, South Road, Durham, DH1 3LE, U.K.

Received December 18, 2003; Revised Manuscript Received February 17, 2004

ABSTRACT: The influence of organic-soluble porogenic solvents (toluene, chlorobenzene, (2-chloroethyl)-benzene, 1,2-dichlorobenzene, and 1-chloro-3-phenylpropane) on the morphology and microstructure of poly(divinylbenzene) emulsion-derived (PolyHIPE) solid foams prepared with a three-component surfactant system is described. It is found that all solvents employed apart from 1,2-dichlorobenzene (C₂B) lead to much higher surface areas than corresponding solid foams prepared with SPAN 80 as surfactant. Experiments where the emulsion droplet phase volume is varied indicate that Ostwald ripening is much reduced with the three-component surfactant system compared to SPAN 80, and this is the likely cause of the higher surface areas. The lesser extent of Ostwald ripening is also suggested by NMR water self-diffusion experiments, which indicate a lower diffusion coefficient when the mixed surfactant is used. The peculiar behavior of C₂B is ascribed to its presumed effect on the packing of surfactant molecules at the interface; the 1,2-substitution pattern may produce a strong steric effect, thus allowing greater contact between the aqueous and organic phases.

Introduction

In the preceding article,¹ the influence of oil-soluble porogenic solvents (toluene, T; chlorobenzene, CB; (2-chloroethyl)benzene, CEB; 1-chloro-3-phenyl propane, CPP; 1,2-dichlorobenzene, C₂B) on the morphology and microstructure of emulsion derived (PolyHIPE) solid foams prepared with the nonionic surfactant SPAN 80 was described. This work was an extension of earlier seminal work by Sherrington and co-workers.² It was found that the surface areas of the solid foams varied according to the solubility parameters of the solvents employed, however the relationship was not simple and values depended on the interfacial and polar properties of the solvents, as well as the solid foam porosity. In addition, the surface areas found were significantly lower than values for resins prepared from the polymerization of mixtures of DVB 80% with each of the solvents under investigation. This indicated that the large amount of water present in the emulsions used to prepare the solid foams was influencing the development of the poly(DVB) network. Investigations indicated that solvents which were adsorbed to a lesser extent at the emulsion interface were poor at preventing the process of Ostwald ripening, where droplet phase (i.e., water) molecules migrate from small droplets through the continuous phase into large droplets. The result of this was a larger concentration of water in the continuous (organic) phase, which served to make the medium a poorer solvent for the developing poly(DVB) network. This caused phase separation to occur earlier in the polymerization, producing larger microgel particles and thus a lower surface area. It was suggested that a more robust interfacial film may reduce the tendency for water molecules to migrate between droplets and thus increase the surface areas of the resulting solid foams. To prepare more stable emulsions and to exploit as

much as possible the porogenic properties of T, CB, and C₂B, we searched in the literature for a surfactant system more efficient than SPAN 80.

The effectiveness of a mixture of an anionic, or cationic, surfactant with an amphiphilic compound for emulsion stabilization has been known for a long time.³ The interfacial film made by this mixture of surfactants shows an increased ability to withstand the pressure of droplet contacts (to prevent coalescence) and to act as a barrier to the passage of the dispersed phase into the continuous phase (to limit Ostwald ripening). It has been discovered that the two surfactants together reduced the interfacial tension to very low values (~ 0.1 mN m⁻¹), much lower than each of them separately.⁴ Emulsions containing a two-surfactant system remain mobile at low total concentration of the surfactants but become semisolid at higher concentration ($\sim 10\%$ or less of the total weight of the emulsion). The surfactants, in fact, associate into a mixed bilayer and form a lamellar phase, which coexists with oil and water in a three-phase equilibrium. This process, whereby the agent that stabilizes the emulsion also controls the consistency over a wide range of values, is referred to as self-bodying action. The essential feature of this self-bodying action is the introduction of a significant viscoelastic component into the rheological behavior of the emulsions.⁵

Hallworth et al.,⁶ as early as 1972, recognized that long paraffin chains can associate with the hydrocarbon chains of alkyl sulfates and thus can be held at the interface. Because of this association, the film will be very coherent and will prevent coalescence of oil droplets. The patent literature⁷ describes the use of a mixture of nonionic, anionic, and cationic surfactants: sorbitan monolaureate (SPAN 20), dodecylbenzene-sulfonic acid sodium salt (DDBSS), and cetyltrimethylammonium bromide (CTAB). This mixture of surfactants is claimed to stabilize emulsions more effectively than SPAN 80. For instance, using a surfactant concentration of less than 10% it is possible to prepare HIPEs at elevated temperatures (≥ 100 °C) without

* Corresponding author. E-mail: n.r.cameron@durham.ac.uk.

[†] Present address: Dipartimento di Chimica, Università degli Studi di Roma, "La Sapienza", P.le A. Moro 5, 00185 Rome, Italy.

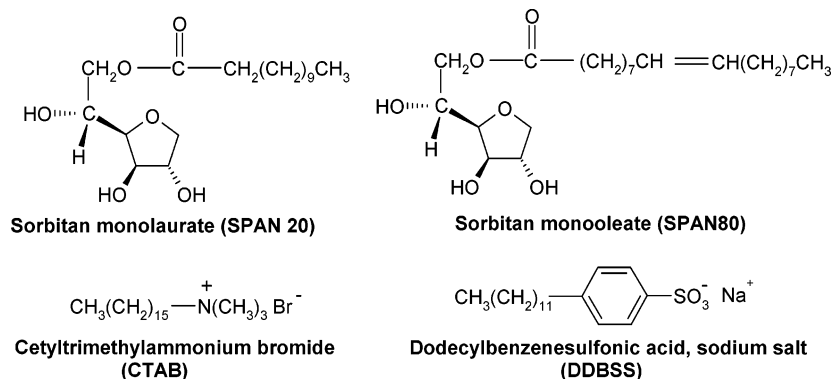


Figure 1. Structures of the surfactants used.

inducing any water-phase separation. This three-component surfactant system offered the possibility of influencing the microporosity of PolyHIPE solid foams prepared with porogens, by reducing or preventing Ostwald ripening.

Experimental Section

Materials. Divinylbenzene (Aldrich; 80 vol % *m*- (55 vol %) and *p*-divinylbenzene (25 vol %), the remainder being *m*- and *p*-ethylstyrene) was purified by passing through a column of basic alumina (Brockmann I) to remove the inhibitor (*p*-tert-butylcatechol). Toluene (T), chlorobenzene (CB), (2-chloroethyl)benzene (CEB), 1,2-dichlorobenzene (C₂B), 1-chloro-3-phenylpropane (CPP) (Aldrich), potassium persulfate (Aldrich), and calcium chloride dihydrate (Avocado) were used as supplied. The surfactants used (all supplied by Aldrich) are listed in Figure 1.

PolyHIPE Preparation. The solid foams prepared were nominally 75, 85, 90, and 92% porous, based on the aqueous phase content. The preparation procedure is described elsewhere.⁸ Briefly, the emulsions were obtained by adding dropwise an aqueous solution of CaCl₂·2H₂O (1.11wt %) and potassium persulfate (0.22wt %) to the organic phase, made of DVB 80% and either SPAN 80 (20 vol % relative to total monomer plus porogen volume) or a mixture of SPAN20, DDBSS, and CTAB (6.3, 0.4, and 0.3 wt %, respectively, relative to total monomer plus porogen weight), under stirring. The polymerization was carried out at 60 °C in an oven for 48 h. The solid foams were extracted with water then 2-propanol for 24 h each in a Soxhlet apparatus. Solid foams were then dried under vacuum at 50 °C to constant mass.

PolyHIPE Coding System. The code system used for designating the PolyHIPE solid foams is the same as that described in the previous paper. The only difference concerns the use of the abbreviation S20AD to indicate the mixture of surfactants, which avoids any confusion when comparison is made between solid foams of the same composition but differing in the type of surfactant used. In the following discussion, solid foams derived from emulsions containing SPAN 80 will be indicated generically with the abbreviation S80.

Surface Area/Pore Size Distribution. Nitrogen adsorption/desorption measurements were performed at 77.3 K on a Micromeritics TriStar 3000 model. Samples were degassed at 100 °C overnight under vacuum prior to data collection. Surface area measurements utilized a nine points adsorption isotherm collected over 0.05 to 0.20 *P*/*P*₀ and analyzed via the BET method.⁹ For each sample a minimum of six determinations were carried out and results are expressed as averages with the associated standard deviations. The average pore size distributions utilized a 53-point adsorption isotherm and were analyzed via the BJH method in accordance with the British Standards Institution.¹⁰ Micropore volumes and areas were evaluated with the *t* plot method.

Mercury Porosimetry. Mercury porosimetry analysis was performed by using a Micromeritics AutoPore III 9420. Samples

were outgassed under vacuum at room temperature for 30 min before intrusion. Intrusion and extrusion mercury contact angles of 130° were used; measurements were conducted according to the set-time equilibration mode. Penetrometers with a stem volume of 1.1310 mL were used. The intrusion volume always comprised between 50 and 85% of the stem volume. Intrusion pressures never exceeded 200 psi (1.38 MPa) in order to avoid any specimen compression.

Electron Microscopy. A Hitachi S2400 electron microscope operating at 25 kV was used for studies of the morphology of the samples. Prior to analysis, specimens were sputter coated with a thin layer of gold to enhance conductivity. Samples for TEM were fixed in 1% aqueous OsO₄ solution and dehydrated in a graded series of alcohols and then embedded in Emix (medium) Resin TO28 (TAAB Laboratories Equipment Ltd.). Curing of the resin was carried out for 36 h at 60 °C. Ultrathin sections (90 nm) of the resulting composite were cut using a Diatome 45 diamond knife (TAAB Laboratories Equipment Ltd.) on a Ventana (RMC) MT-XL Ultramicrotome (Ventana Medical System Inc.). The sections were mounted on uncoated 400 mesh copper Gilder grids G400, of 3.05 mm diameter. The grids were examined using a Philips CM100 (compustage) transmission electron microscope (TEM) operated at 100 kV. Micrographs were recorded at magnifications of 380, 4600, and 10 500×. Micrographs taken at 380× were used for the evaluation of the average cavity and interconnecting window diameters. Such measurements were carried out using the instrument software on a significant number of voids (typically, a few hundred) in order to give statistical relevance to the figures produced.

Solid-State ¹³C NMR. Solid-state ¹³C NMR spectra were recorded on a Varian Unity Inova spectrometer with a 7 mm rotor (Doty Scientific MAS probe). The spectra were obtained using a direct polarization experiment with proton decoupling during acquisition at a frequency for ¹³C of 75.43 MHz. A 90° excitation pulse (duration 5 μs) was used with a 30 s recycle delay, at a spin rate of 7800 Hz. 2200 repetitions were accumulated, with an acquisition time of 15 ms. Spectral referencing was to an external sample of (CH₃)₄Si. Calculated and deconvoluted spectra were obtained using the on-board Varian NMR software.

Determination of the Diffusion Coefficient of Water in Emulsions Using ¹H NMR. The self-diffusion of water was measured using a 500-MHz Varian Unity Inova 500 narrow bore spectrometer equipped with a Performer II gradient pulse amplifier and an actively shielded 5 mm indirect detection probe capable of producing up to 30 G cm⁻¹ *z* field gradient pulses. Automated *z* gradient shimming based on deuterium spin echoes was used. The temperature for all measurements was 25 ± 0.1 °C. Water diffusion coefficients were measured using a pulse sequence incorporating pulsed-field gradients such as the bipolar pulse pair stimulated echo (BPPSTE) pulse sequence. Diffusion coefficients are obtained from BPPSTE spectra by monitoring signal attenuation as a function of the applied magnetic field gradient amplitude and fitting eq 1 to the experimental results

$$I = I_0 \exp[-D(\gamma\delta G)^2(\Delta - (\delta/2) - (\tau/3))] \quad (1)$$

where I is the resonance intensity measured for a given gradient amplitude, G , I_0 is the intensity in the absence of the gradient pulse, γ is the gyromagnetic ratio, δ is the duration of the bipolar gradient pulse pair, Δ is the diffusion delay time, and τ is a short gradient recovery delay time during which relaxation and spin–spin coupling evolution are not significant.

Results and Discussion

To compare the effectiveness of the mixture of surfactants in preventing Ostwald ripening and partitioning in the precursor emulsions leading to PolyHIPEs, the same set of DVB 80%, PV90, and PolyHIPE solid foams as described in the previous paper, including in their initial emulsion formulation one of the porogens T, CB, C₂B, CEB, and CPP, was prepared. The characterization of the resulting solid foams was carried out as previously discussed.¹ In Figure 2, SEM micrographs of X80PV90(1Por)S20AD type solid foams are shown. All solid foams exhibit, with the exception of X80PV90-(1CEB)S20AD (X80PV90(1CPP)S20AD has a very similar morphology and its SEM micrograph is not shown), a well-defined morphology. Solid foams prepared with CEB and CPP as porogens show a heterogeneous morphology: portions of the solid foam are characterized by a continuous wall structure; others, on the contrary, show evidence of wall break up. The void size is comparable to those of the other solid foams (Figure 2a–c), but it seems that the size of interconnecting holes is higher in relation to void size.

It is useful at this point to make a comparison with the morphology of the corresponding S80 type solid foams.¹ In that case the morphology of solid foams prepared with T and CB was characterized by a continuous polymeric framework, that prepared by employing C₂B showed some sign of wall break up whereas this was very evident in the case of X80PV90(1CEB/CPP)-S80 solid foams. When the mixture of surfactants is used, changes in morphology accompanying the use of the different porogens are much less pronounced. For instance X80PV90(1C₂B)S20AD is better textured than X80PV90(1C₂B)S80 (previous paper, Figure 5e), its morphology being characterized by a continuous polymeric framework. Pronounced variations in morphology are still met when CEB and CPP porogens are used but to a lesser extent than those in the corresponding S80 solid foams. Macroscopically, solid foams depicted in Figure 2 are tougher than the corresponding S80 analogues and are not chalky. In this respect, there are not any discernible differences between the first three solid foams of Figure 2a–c. On the contrary, those prepared by employing CEB (Figure 2d) and CPP as the porogens are weaker than the other solid foams.

All these observations allow us to infer that when the mixture of surfactants is used, the abilities of the porogens to coadsorb with the primary surfactant at the O/W interface are reduced and this might be a consequence of a more coherent surfactant interfacial film which limits porogen coadsorption. SPAN 80, because of its chemical structure (a cis double bond in its hydrocarbon tail) allows porogen molecules to insert in the space between adjacent surfactant molecules adsorbed at the interface. This capability is evidently attenuated when the mixture of surfactants is used.

Following the same protocol of solid foam analysis as was used with S80 solid foams (see previous paper), the

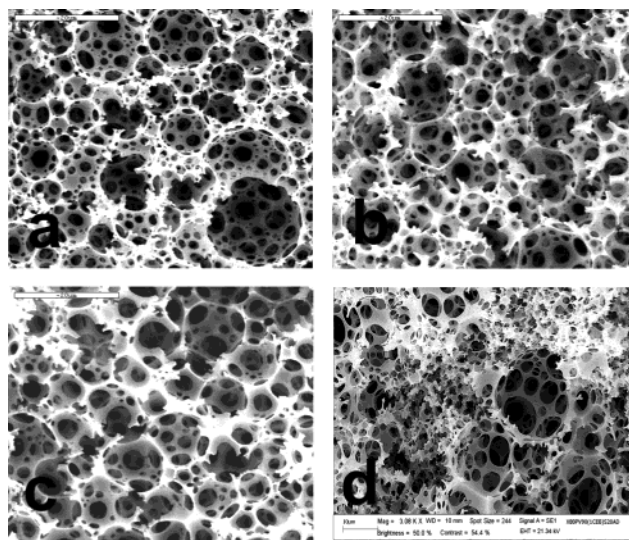


Figure 2. SEMs of PolyHIPEs prepared with the following porogens: (a) T; (b) CB; (c) C₂B; (d) CEB. Surfactants used: SPAN 20, DDBSS, and CTAB. Scale bar = 20 (a–c) and 10 (d) μ m.

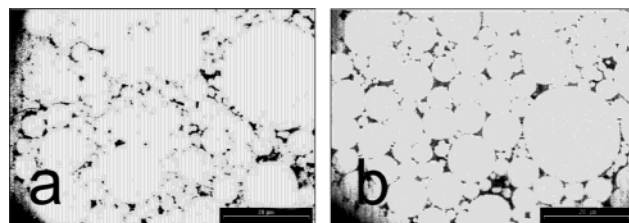


Figure 3. TEMs of PolyHIPE solid foams: (a) X80PV90(1T)-S20AD; (b) X80PV90(1CB)S20AD. Scale bar: 20 μ m.

quantitative determination of void and interconnecting hole average diameters was carried out using TEM micrographs, two examples of which are reported in Figure 3. The emulsions containing the mixture of surfactants were relatively viscous, especially at high values of the W/O ratio. In fact, the qualitative inspection of TEM micrographs (Figure 3, parts a and b) shows the presence of a plurality of voids of different dimensions, from very small (1 μ m) to relatively large (30 μ m). As the W/O ratio increases the emulsion becomes more viscous and the shear rate provided by the stirring becomes less efficient in comminuting the added water phase. The final solid foam is then characterized by a more polydisperse void size distribution. This effect has been described also by Tai et al.¹¹ Qualitatively, cavities are, on average, separated by a thinner layer of polymeric material than in S80 analogue solid foams (compare Figure 3, parts a and b, and Figure 3 in the previous paper). Values of void, $\langle D \rangle$, and interconnecting window diameter, $\langle d \rangle$ (Table 1), are systematically lower (about one-half) than those of the corresponding S80 solid foams.¹ Values referring to X80PV90(1CEB/CPP)-S20AD are omitted because the presence of areas of strut type morphology prevented the determination of reliable averages. Quantitative estimation of the ratio $\langle d \rangle / \langle D \rangle$ confirms the qualitative observation reported above concerning the thickness of the polymeric layer surrounding voids. $\langle d \rangle / \langle D \rangle$ values are significantly lower than those of the corresponding S80 solid foams. This implies that the lowering of interfacial tension is more pronounced when the mixture of surfactants is used as compared to the situation in which SPAN 80 was used as a surfactant.

Table 1. Characterization of PolyHIPE Solid Foams

sample	$\langle D \rangle$ (μm) ^a	$\langle d \rangle$ (μm) ^b	$\langle d \rangle / \langle D \rangle$	$\langle \Delta \rangle$ (μm) ^c	V_p (cm ³ g ⁻¹) ^d
1 X80PV75(1CB)S20AD	3.9	1.3	0.32	2.8	5.4
2 X80PV85(1CB)S20AD	2.7	1.2	0.43	2.5	10.5
3 X80PV90(1CB)S20AD	4.4	2.4	0.55	3.7	13.7
4 X80PV92(1CB)S20AD	6.9	4.3	0.62	—	—
5 X80PV90(1T)S20AD	4.7	2.9	0.60	—	—
6 X80PV90(1C ₂ B)S20AD	6.6	3.4	0.51	—	—

^a Average void diameter (determined by TEM). ^b Average window diameter (determined by TEM). ^c Relative average window diameter (determined by Hg intrusion porosimetry). ^d Pore volume determined from pore size distributions obtained with Hg porosimetry.

The results displayed in Table 1 seem to indicate that the degree of interconnection, $\langle d \rangle / \langle D \rangle$, when considered as a function of porogen polarity and hydrogen-bond-forming abilities, follows a reversed order with respect to that observed with S80 solid foams. In the latter type of solid foams, as the polarity of the porogens increases, the degree of interconnection increases. On the contrary, in the case of S20AD-type solid foams, the reverse dependence is observed. This means that, instead of enhancing the interfacial excess (as in the case of S80 solid foams), the increase in porogen polarity leads to surfactant depletion at the interface.

In Table 2, the surface area and porosity data of the solid foams prepared with T, C₂B, CEB, and CPP as the porogens are reported. V_p is the cumulative pore volume determined by N₂ adsorption and $\langle D_w \rangle$ is the average diameter of pores within the walls of the solid foams. The surface area of X80PV90(1T)S20AD (entry 1) is as high as 720 m² g⁻¹ and this is indeed a remarkable result, especially if these data is compared with the surface area of the resin obtained by bulk polymerization of DVB 80% in the presence of T (760 m² g⁻¹, see preceding paper). The difference in their surface areas is only 5%. The same comparison for the other solid foams and corresponding resins shows that this difference increases in the following order: T(5%) < CB(12%) < CEB \approx CPP (16%) < C₂B (48%). In the case of the 1:1 mixture of CB and CEB porogens, the inclusion of the mixture of surfactants (Table 2) in the emulsion formulation increases its surface area only slightly (~ 50 m² g⁻¹) over X80PV90(0.5CB + 0.5CEB)S80 (570 m² g⁻¹).⁸ This confirms that CEB is itself a good cosurfactant. Pore volumes as well as the average pore diameter, with the exception of X80PV90(1C₂B)S20AD, are basically constant. Also, the percentage contributions of micropores (<2 nm)¹² to total surface areas and pore volumes are at a level comparable with that observed for the macroporous resins.¹ As has been said above, X80PV90(1C₂B)S20AD represents an exception when compared to the other solid foams: its N₂ sorption results indicate that, in the presence of the mixture of surfactants, the solvent medium in which polymerization is taking place is slightly worse than in the presence of SPAN 80. Table 2 includes the N₂ sorption data of a solid foam (entry 10) obtained using DVB 55%. The comparison of its surface area with that of X80PV90(1CB)S80 (346 m² g⁻¹, see previous paper) shows the influence of partitioning of the porogen, and, in particular, water diffusion through the continuous phase, on the quality of the organic medium in which polymerization is taking place. Despite a lower cross-linking density, the surface area of X55PV90(1CB)S20AD is 20% higher than that of X80PV90(1CB)S80.

Examples of the N₂ sorption isotherm type and pore size distribution encountered with X80PV90(1Por)-S20AD solid foams are displayed in Figure 4, parts a and b, respectively. All pore size distributions with the exception of X80PV90(1C₂B)S20AD are very close to each other, which is indicative of uniformity of microstructure. Isotherms are all of type II and exhibit a H4 hysteresis loop type as opposed to the type II isotherm and H3 loop exhibited by solid foams belonging to the X80PVN(1CB)S80 series.⁸ In that case, the adsorption and desorption curves were parallel over almost the whole range of gas uptake whereas in the case of X80PV(1Por)S20AD solid foams the isotherms show a wider hysteresis loop instead of nearly retracing the adsorption curve. The occurrence of a wider, more-pronounced hysteresis loop indicates that evaporation from a pore is a distinctly different process from condensation within it. When gas condenses in a pore, the condensate builds from the wall inward toward a central core of decreasing diameter. However, it must evaporate from a liquid surface with a quite different curvature. This inhibits the evaporation and causes the decreasing portion of the loop to lag behind until all pores have emptied.¹³ Thus, the width of the hysteresis loop is related to the size of pores: the smaller the pores the higher is the radius of curvature of the liquid/gas interface and the higher is the difference of pressure across the interface. The wider hysteresis loops exhibited by X80PV90(1Por)S20AD solid foams are in accordance with the size distributions being shifted more toward a lower pore size and characterized by a lower proportion of macropores (>50 nm) than those of X80PV90(1Por)S80 solid foams. The pore size distribution reported in Figure 4b shows that in the case of X80PV90(1C₂B)S20AD the proportion of mesopores is significantly less than all the other solid foams, of which X80PV90(1T)S20AD is an example.

To quantify better the effectiveness of the mixture of surfactants in minimizing Ostwald ripening, a useful test is to study the influence of PV on solid foam porosity. PV is strictly correlated with the term $f(\phi)$ of the Ostwald ripening rate equation (see preceding paper), which is a measure of the interaction among diffusion domains. SPAN 80 proved to be quite ineffective in preventing Ostwald ripening and as a result the surface areas of X80PVN(1CB)S80 solid foams showed a marked dependence on PV. Accordingly, X80PVN(1CB)S20AD solid foams where $N = 75, 85, 90$, and 92 were prepared and their morphology was examined by SEM and TEM and porosity by N₂ sorption and mercury intrusion porosimetry.

SEM micrographs (Figure 5) show morphological characteristics consistent with a droplet packing in the precursor emulsions dictated by PV. At low PV (75 and 85%) the droplets of the dispersed phase enjoy a relatively high degree of freedom in terms of size and relative position. On polymerization, a solid foam with more polydisperse void and interconnecting hole sizes is produced (Figure 5, parts a and b). At higher PV (90 and 92%), the droplets of the dispersed phase are more densely packed, and as a consequence, the resulting solid foams are characterized by more homogeneous void and interconnecting hole sizes. In particular, in the PV92 solid foam the walls are rather thin as a result of the high W/O ratio and this solid foam has clearly suffered some damage during the purification procedure. The trend outlined above is clearer when void and

Table 2. Surface Areas, Cumulative Pore Volumes, Average Pore Diameters, Micropore Pore Volumes, and Micropore Areas of DVB 80% PolyHIPE Solid Foams

	sample	surface area (m ² /g) ^a	V_p (cm ³ /g) ^{b,c}	$\langle D_w \rangle$ (nm) ^{b,c}	micropore vol (cm ³ /g) ^d	micropore area (m ² /g) ^d
1	X80PV90(1T)S20AD	721 ± 12	0.81 ± 0.02	4.39 ± 0.05	0.019 ± 0.006	66 ± 11
2	X80PV90(1CB)S20AD	689 ± 15	0.80 ± 0.03	4.36 ± 0.08	0.018 ± 0.003	64 ± 6
3	X80PV90(1C ₂ B)S20AD	435 ± 28	0.56 ± 0.03	5.4 ± 0.2	0	0
4	X80PV90(1CEB)S20AD	665 ± 21	0.81 ± 0.04	4.70 ± 0.04	0.014 ± 0.004	53 ± 9
5	X80PV90(1CPP)S20AD	660 ± 7	0.79 ± 0.01	4.60 ± 0.02	0.006 ± 0.001	37 ± 2
6	X80PV75(1CB)S20AD	680 ± 18	0.76 ± 0.04	4.32 ± 0.04	0.016 ± 0.003	56 ± 7
7	X80PV85(1CB)S20AD	684 ± 5	0.770 ± 0.007	4.26 ± 0.08	0.018 ± 0.003	62 ± 6
8	X80PV92(1CB)S20AD	640 ± 7	0.710 ± 0.004	4.19 ± 0.04	0.018 ± 0.003	61 ± 5
9	X80PV90(0.5CB)S20AD	351 ± 18	0.35 ± 0.05	3.90 ± 0.07	0.008 ± 0.002	31 ± 8
10	X55PV90(1CB)S20AD	446 ± 31	0.58 ± 0.03	5.2 ± 0.2	0.0011 ± 0.0009	20 ± 3
11	X80PV90(0.5CB + 0.5CEB)S20AD	634 ± 21	0.67 ± 0.02	4.61 ± 0.08	0.0020 ± 0.0005	28 ± 9

^a From BET treatment of N₂ adsorption data. ^b See text for definition of terms. ^c From BJH treatment of N₂ adsorption data. ^d From *t* plot.

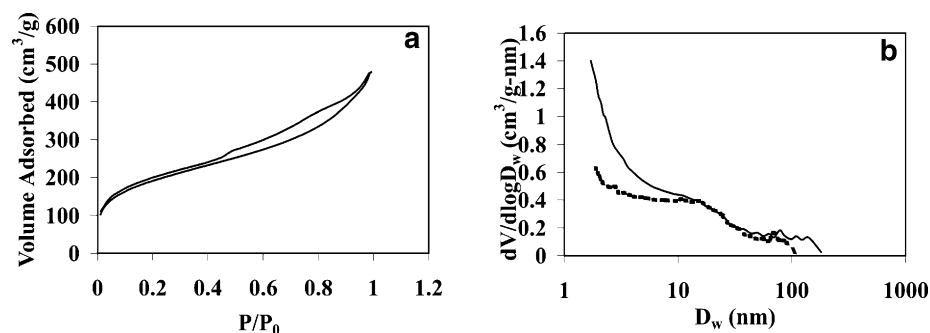


Figure 4. (a) Example of N₂ isotherm encountered with solid foams listed in Table 2. (b) Pore size distribution (BJH) of X80PV90-(1T)S20AD (full line) and X80PV90(1C₂B)S20AD (dashed line).

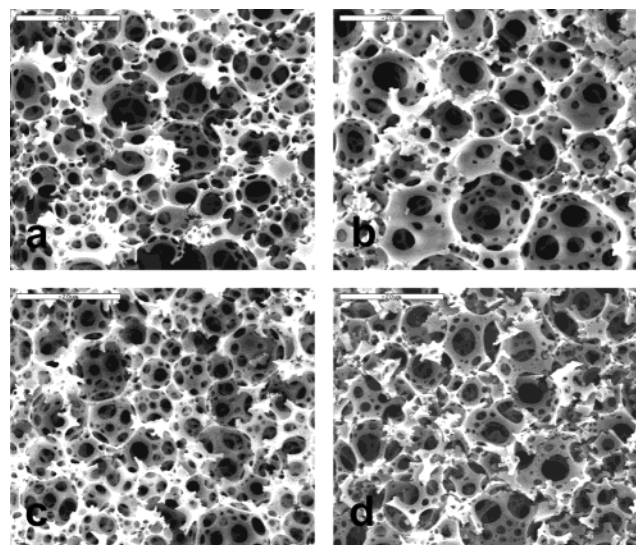


Figure 5. Scanning electron micrographs of PolyHIPE solid foams characterized by increasing PV: (a) PV75; (b) PV85; (c) PV90; (d) PV92. Porogen used: CB. Surfactants used: SPAN 20 plus DDBSS and CTAB. Scale bar = 20 μm.

interconnecting hole average diameters are considered. These data are obtained from TEM micrographs and are displayed in Table 1. In agreement with the data previously described for X80PV90(1Por)S20AD, void and interconnecting hole average diameters of the X80PVN-(1CB)S20AD solid foams are about half those of the corresponding solid foams prepared with SPAN 80. Furthermore, comparison of the $\langle d \rangle$ values between the two set of solid foams shows that the size of the interconnecting windows is proportionally larger relative to void size for solid foams prepared from the mixed surfactant system, and the degree of overlapping as

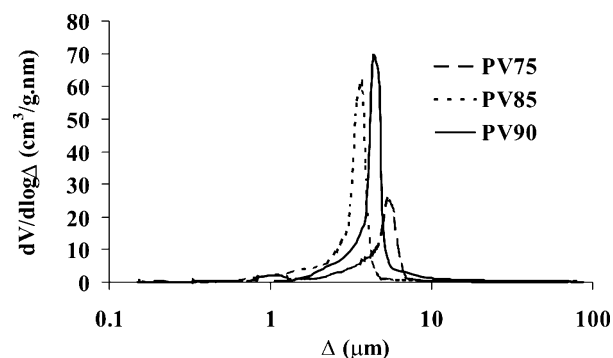


Figure 6. Intrusion mercury porosimetry pore size distribution of DVB 80% PolyHIPE solid foams prepared using CB as a porogen, SPAN 20, DDBSS, and CTAB, as surfactants and characterized by increasing pore volume.

expressed by the ratio $\langle d \rangle / \langle D \rangle$ indicates that the films of the continuous phase surrounding droplets in the precursor emulsions are thinner. All these observations point to a more pronounced reduction of the interfacial tension caused by the mixture of surfactants than that promoted by SPAN 80.

Intrusion mercury window size distributions are displayed in Figure 6. The distribution curve referring to X80PV92(1CB)S20AD solid foam has been omitted on purpose because the material was not sufficiently tough to survive the analysis and did not yield any reproducible results. Values of the average interconnecting hole diameters (Δ) and relative pore volumes are reported in Table 1. In the case of PV 75 the distribution curve shows the presence of a main peak at 5.4 μm and a small one at 1.0 μm. PV 85 and 90 distribution curves are monomodal with peaks placed at 3.7 and 4.4 μm. The presence of two peaks is indicative of a rather polydispersed window size distribu-

tion which, as stated previously, is the outcome of a relatively low W/O ratio. It is also quite evident from comparison of the distribution curves that the range of diameters covered by the PV 85 curve is larger than the PV 90 one. Comparison between the ratios of intrusion volumes and the ratios of the volumes of dispersed phase for the pairs PV 85 and 75 and PV 90 and 85 reveals that the first two solid foams did not suffer any compression (≈ 1.9 is the ratio between the two quantities) while PV 90 underwent some collapse as witnessed by the intrusion volumes ratio being 1.3 vs a theoretical one of 1.6. The latter value is slightly higher than the one found for the PV90/PV85 S80 solid foams (1.1, see previous paper) and these data together with the evidence of thinner solid foam walls (see $\langle d \rangle / \langle D \rangle$ values, Table 1) provides a clear indication that the mechanical properties of the S20AD solid foams are better than the corresponding S80 solid foams.

Surface area for the series of solid foams characterized by an increasing PV are reported in Table 2. Comparison with the results concerning the equivalent S80 solid foams shows that the surface areas of the S20AD PVN solid foams are much higher, the difference increasing with PV. This is a consequence of the lack of variation of porosity with PV in the case of S20AD type solid foams. The only decrease in surface area is very small (7%) and occurs for PV 92 compared to PV < 92. On the contrary, in the case of X80PVN(1CB)S80 solid foams, surface areas and porosities were approximately constant for PV 75 and 85 but decreased markedly when PV > 85. When the mixture of surfactants replaces SPAN 80, the porosity data are constant for PV 75, 85, and 90 and are 45% higher than PV 75 and 85, and about 170% for PV 92, S80 type solid foams. The invariance of surface area and porosity data indicates that Ostwald ripening has been drastically reduced. For instance, surface area decreases only slightly when PV exceeds 90% and those referring to 85 and 90 PV are the same. This set of data, together with that regarding the difference between DVB(CB) and X80PV90(1CB)-S20AD, offers a quantitative measure of the effectiveness of the mixture of surfactants in preventing Ostwald ripening and partitioning. In Table 2, the surface area of a solid foam characterized by a monomer-to-porogen ratio of 1:0.5 (X80PV90(0.5CB)S20AD, entry 5) is also included. Its surface area is about half that of X80PV90(1CB)S20AD (monomer-to-porogen ratio of 1:1) (entry 3). These results indicate that the diffusion of water has been drastically reduced and that the interfacial film made of the mixture of surfactants effectively screens the organic medium from the aqueous phase, independent of the polarity of the former.

The combined evidence of smaller droplet sizes and a thinner layer of polymeric material separating adjacent voids (Table 2) in solid foams prepared by using the mixture of surfactants suggests that the interfacial tension in the precursor emulsions is lower than in the corresponding ones prepared using SPAN 80. The decrease in droplet size seems not to be as dramatic as that caused by the addition to the organic phase of CEB or CPP in X80PV90(1CEB/PP)S80 emulsions.⁸ From this, we can infer that it is not the lowering of interfacial tension which is mainly responsible for the attenuation of Ostwald ripening. It seems more reasonable to attribute this behavior to the creation, by the mixture of surfactants, of a compact barrier which opposes the

exchange of molecules (water and porogen) between the two phases. In the literature,¹⁴ it has been reported that the presence of an adsorbed gelatin layer reduces the rate of transfer of diethylphthalate across the hexadecane/water interface by a factor of approximately 10^4 compared to the diffusion-controlled rate. Kabal'nov and Shchukin¹⁵ have given equations describing the retardation effect of a membrane at the interface. We have observed experimentally that if an aqueous layer is deposited carefully on top of an organic one containing the mixture of surfactants, a semisolid membrane develops at the interface, while in the case of SPAN 80 the interfacial film of surfactant remains fluid.

Because the mixture of surfactants has proved to be effective in isolating the organic phase from the aqueous one we would expect, simply from a consideration of the solvating power of the porogens used, that the surface areas of X80PV90(0.5CB + 0.5CEB)S20AD and X80PV90(1C₂B)S20AD would be higher or at least equal to that of X80PV90(1CB)S20AD. As can be seen (Table 2), the surface area of the X80PV90(0.5CB + 0.5CEB)-S20AD deviates slightly from that of X80PV90(1CB)-S20AD while that of X80PV90(1C₂B)S20AD is much lower. Also, the difference in surface area between X80PV90(1C₂B)S20AD and DVB(C₂B) (440 and 830 m² g⁻¹, respectively) is particularly relevant (about 47%), which indicates that, in the presence of this porogen, the mixture of surfactants fails to prevent, with the same effectiveness, both diffusion and partitioning. This hypothesis finds some support from the result concerning the use of T as a porogen. In this case, a solid foam (X80PV90(1T)S20AD, Table 2) with the highest surface area is obtained. From these results and those relative to $\langle d \rangle / \langle D \rangle$, it is possible to infer that the nature of porogen and its interaction with the surfactants is again determinant as far as the final solid foam microstructure is concerned.

In Figure 7, the microstructures as determined by electron microscopy of X80PV90(1CB)S80, X55PV90(1CB)S20AD, and X80PV90(1CB)S20AD are reported. SEM micrographs (left column of Figure 7a–c) clearly show that the average dimension of the microgel particles composing the walls of the above solid foams decreases markedly down the series. In particular, X55PV90(1CB)S20AD particles are significantly smaller than those of X80PV90(1CB)S80. TEM micrographs (right column of Figure 7d–f) provide a direct image of the porosity inside the materials. In accordance with the SEM image (Figure 7a) and with $dV/d(\log D_w)$ nitrogen adsorption results,¹ the porous structure in X80PV90(1CB)S80 (pores between agglomerates of particles) is rather heterogeneous, pore diameters occurring over a wide range. The micromorphology as evidenced by electron microscopy of X80PV90(1CB)S80 is compatible with a polymerisation taking place in a less thermodynamically favorable porogen compared to the other two cases in Figure 7.

When the polymerization in the emulsion starts in the presence of a poor solvent for the polymer, the porous texture formation follows a three-stage mechanism.¹⁶ The agglomeration of polymer chains to give nuclei takes place initially, followed by the formation of microspheres and finally agglomerates. Very small pores (50–150 Å) are located between the nuclei, and these pores are mainly responsible for the high surface area. Between the microspheres, there is a second family of intermediate pores (200–500 Å). A third family

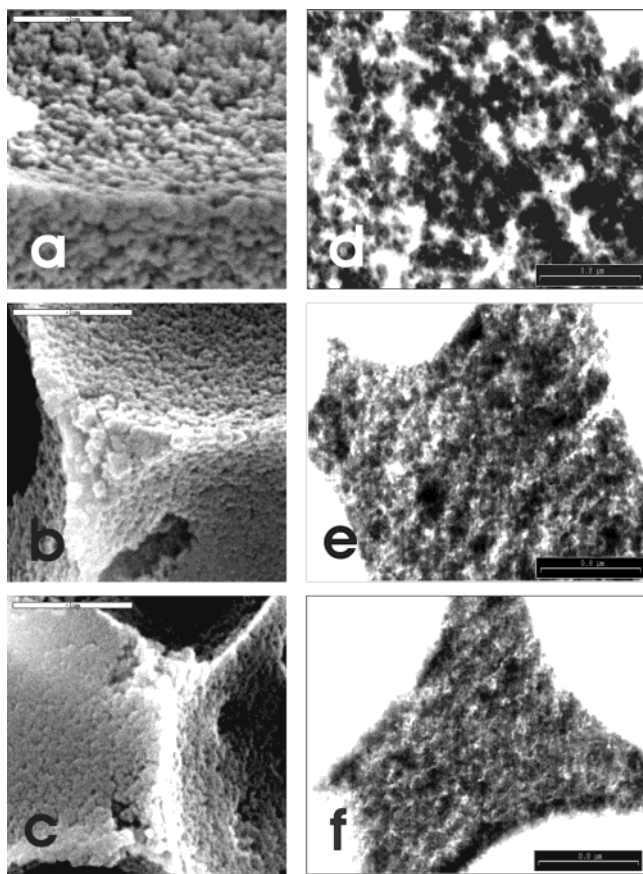


Figure 7. SEM (left column, a–c) and TEM (right column, d–f) of PolyHIPE solid foams: (a and d) X80PV90(1CB)S80; (b and e) X55PV90(1CB)S20AD; (c and f) X80PV90(1CB)-S20AD. Scale bars are 1 μm (a–c) and 0.8 μm (d–f).

of large pores is located between the agglomerates. The resulting porous structure is characterized by a large pore volume with a relatively large pore diameter. During the polymerization, the solvating power of the liquid medium is continuously decreasing because the monomer is consumed, and at a certain point, the solvent medium does not solvate the polymer formed, which precipitates. The separated nuclei preferentially “extract” the monomer from the surrounding liquid polymerization mixture containing the less compatible solvent because the monomer “prefers” the more thermodynamically favorable environment within the nuclei. The enlarged nuclei can also attract and coalesce with the newly precipitated chains and further increase their size. As a result, both large microglobules and large pores are formed.

In the case of X55PV90(1CB)S20AD and X80PV90(1CB)S20AD (Figure 7, parts b and c), the microgel particles are quite small, especially in the latter case where they are at the edge of the resolution limit of the SEM used and are hardly discernible. Their porous structures are therefore much more homogeneous and uniform across the materials. These features are consistent with polymerization occurring in an organic medium which is a good solvent for the polymeric network. In fact, when the polymerization is run in the presence of an inert diluent that is a good solvent for the polymer, two levels of particle substructure instead of three, as discussed previously, are formed. The polymer texture is built up of rather large nuclei (20–50 nm) and agglomerates but not microspheres. The quality of the solvent medium does not change much

during the course of polymerization. Because the polarity within the separated nuclei is not very different from that of the surrounding solution, monomers are not forced to adsorb preferentially into the nuclei and the polymerization proceeds with formation of nuclei that remain individualized. As a result, a larger number of individual nuclei compete for the remaining monomers. This leads to a large number of small microglobules that aggregate thus forming the macroporous structures with fine individual microglobules. The result is an increased microporosity that enhances the internal surface area. The employment of an increasing fraction of cross-linking monomer generally leads to porous structures with larger surface areas and smaller pore sizes. The phase separation takes place at a lower monomer conversion for systems with a high fraction of cross-linker. Both the adsorption of monomers and the coalescence of nuclei are limited as a result of their cross-linking. Thereby, the number of smaller individual nuclei remains large, and smaller microspheres persist.

Since the real level of cross-linking is known to be an important parameter in the generation of the morphology of porous resins,¹⁷ contributing substantially to controlling the point of phase separation of the growing polymer matrix from the porogen, it was thought important to assess the level of unreacted C=C bonds in the solid foams and resins. We have already stressed how the swelling properties of the reaction medium in the continuous phase depended on the nature of the surfactant system employed. When the mixture of surfactant was employed, Ostwald ripening was effectively diminished as compared to the situation in which SPAN 80 was used as a surfactant. We wondered if the quality of the solvent medium had an effect on the degree of conversion of DVB double bonds, which would then influence the gel point and hence contribute to the differences in surface areas observed in pairs of solid foams differing only in the surfactant system used (for instance, X80PV90(1T)S80, X80PV90(1T)S20AD). Furthermore, the knowledge of the chemical composition of the solid foams and resins would allow us to calculate the solubility parameter of poly(DVB) and to compare it with those of the porogens employed. To this end, quantitative ¹³C solid-state NMR was employed in order to obtain an estimation of the level of unreacted double bonds. Examples of the spectra obtained are shown in Figure 8, parts a and b.

In part a is reported the experimental spectrum, showing the ppm position of peaks. In part b, the deconvoluted peaks and the calculated spectra are reported. The peak assignments are illustrated together with the chemical structure in Figure 9.

The degree of unreacted double bonds was found to be about 35% independent of the surfactant system, polymerization mode and nature of the porogen used. This means that the quality of the solvent medium determines pore structure directly through the point of gelation and not via the degree of conversion of double bonds. Quantitative estimation of the degree of cross-linking in PolyHIPE solid foams made from DVB 80% allowed the calculation of its cohesion solubility parameter and of its components by employing the Hoy approach:

$$\bar{\delta}_i = \phi_1\delta_{1i} + \phi_2\delta_{2i} + \cdots \phi_n\delta_{ni} \quad (2)$$

where ϕ represents the volume fractions and the index, i , the type of dispersive interaction (d, p, and h).¹⁸ The

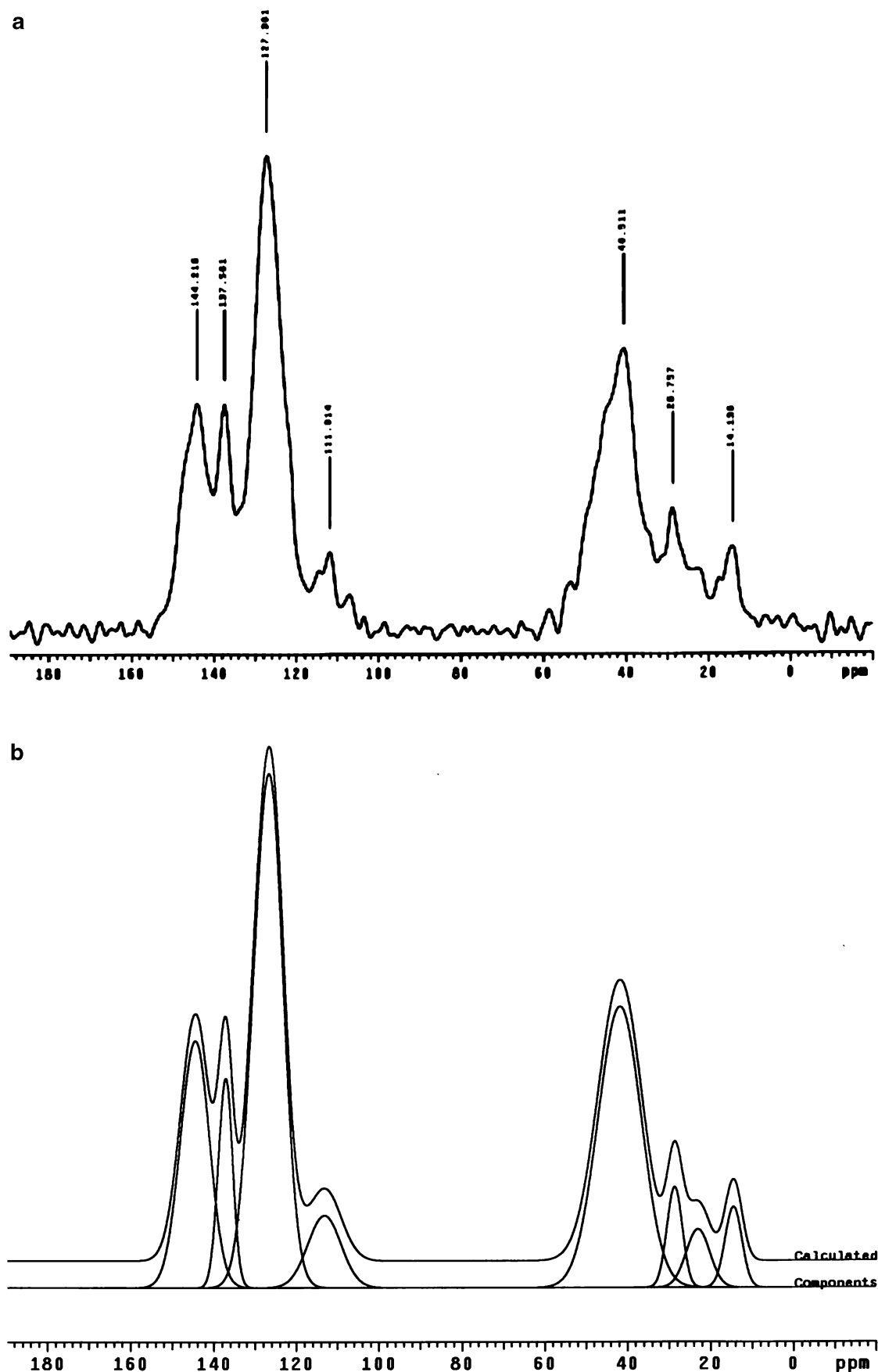


Figure 8. ^{13}C Solid-state SPE NMR spectra of dry poly(DVB 80%)HIPE: (a) experimental spectrum; (b) deconvoluted and calculated spectra.

solubility parameter δ calculated in this manner was found to be $20.5 \text{ (MPa)}^{1/2}$. Even if this result must be

considered with caution because of the uncertainty inherent in the method of calculation and experimental

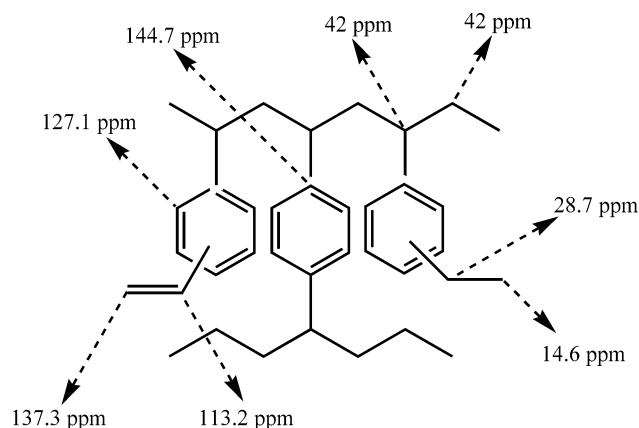


Figure 9. Peak assignments of the ^{13}C solid-state NMR spectra of poly(DVB 80%).

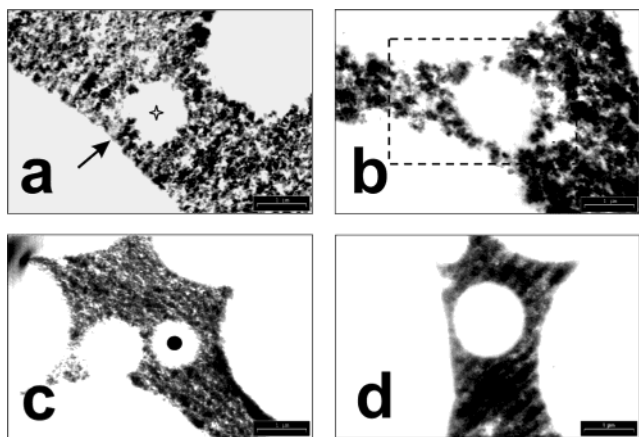


Figure 10. TEMs showing details of droplets morphology of PolyHIPE solid foams: (a) X80PV75(1CB)S80; (b) X80PV92(1CB)S80; (c) X80PV90(1CB)S20AD; (d) X80PV90(1T)S20AD. Scale bar: 1 μm .

error, the agreement between this value and that found experimentally for C_2B ($20.5 \text{ (MPa)}^{1/2}$) is striking.

TEM micrographs, Figure 10, provide direct evidence that the porous structure of the walls of the solid foams is determined mainly (partitioning of the porogen between aqueous and organic phases can also, to some extent, play a role) by diffusion of water through the continuous phase.

In finite volume fraction systems, the detail of the spatial distribution of the droplets plays a role in determining the ripening behavior of the system. This is seen by considering the difference in interfacial solubilities (S_1 , S_2) between two droplets of different size (r_1 , r_2), as expressed by the Gibbs–Thomson equation, eq 3,

$$\ln \frac{S_1}{S_2} = \frac{\gamma^i V_m}{RT} \left(\frac{1}{r_1} - \frac{1}{r_2} \right) \quad (3)$$

(γ^i is the interfacial tension between the two phases and V_m is the molar volume) and the distance between these two particles. For example, if a small droplet is located near a large droplet, it will have a larger dissolution rate than when it is located at the same distance from a droplet of nearly the same size, since in the former case the interfacial concentrations of the droplets are quite different, whereas in the latter case the interfacial concentrations of both droplets are nearly the same. In a finite volume fraction system, droplets of the same

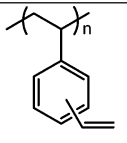
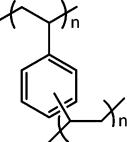
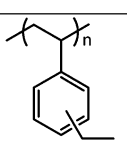
size will coarsen at different rates depending on the local distribution of the other droplets in the system. Inter-droplet diffusional interactions can also influence the morphologies of the coarsening domains. Even under the assumption of isotropic interfacial energy, the droplets may not possess the spherically symmetric morphology assumed in the LSW theory¹⁹ but instead a shape that is related to the strength of the local interparticle diffusional interactions.

In the present case it must be remembered that the morphology of the solid foam is a replica of the emulsion structure at the gel point and its features result from processes taking place in the emulsion. Hence, small droplets undergoing the ripening process are surrounded by a diffusion layer characterized by a concentration gradient fading out as the distance from the droplet surface increases. As the concentration of water is higher in the layers of continuous phase adjacent to the droplets surface, the porosity of the solid foam near the surface of cavities should be locally coarser than in the bulk because there, the quality of the solvent is worse.

From TEM micrographs reported in Figure 10, parts a and b, it is evident that the symmetry of the small droplets (such as the one of about 1 μm in diameter indicated with a star in Figure 10a) deviates remarkably from spherical, showing the presence of branches protruding out from the cavity surface. On the contrary, much larger voids (such as the one indicated with an arrow in Figure 10a) have much smoother surfaces. The rate at which Ostwald ripening occurs is affected by the distance between the droplets since the dispersed material must be transported between them. Hence, this process will be accelerated when droplets are more densely packed.²⁰ The volume fraction dependence is included in LSW theory simply as a multiplication factor $f(\phi)$. A number of theoretical studies^{21,22} have examined $f(\phi)$. Analytical solutions are not available, hence only numerical solutions have been proposed. The most discussed of these has been the theory of Enomoto et al.²² The rate is predicted to increase by a factor of 2.5 in the range $\phi = 0.01$ –0.3.

The difference in surface areas encountered in the series X80PVN(1CB)S80¹ may reflect the dependence of diffusion rates on $f(\phi)$. To what extent this phenomenon is responsible for the differences in surface areas is difficult to evaluate. In the literature, there are neither theoretical studies nor experimental results concerning the influence of the volume fraction of the dispersed phase on Ostwald ripening rates in the range of the high values of ϕ characteristic of concentrated emulsions ($\phi \geq 0.74$). Comparison of the details of the morphology of small voids, and of the porous structure in the portion of the solid foam surrounding them, between solid foams characterized by PV 75 and 92 allows some differences to be discerned. For instance, in the case of X80PV92(1CB)S80 (Figure 10b) the porosity of the solid foam in the proximity of the surface of small voids tends to be coarser and to span longer distances when compared to those of X80PV75(1CB)S80 (Figure 10, parts a and b). Also, solid foam porosity enclosed in harbors surrounded by three or more voids clearly shows features arising from droplet interactions in the precursor emulsion. This is likely to be the result of an increased interaction between diffusion spheres of neighboring droplets. When the mixture of surfactants is used, as in the case of X80PV90(1CB)S20AD

Table 3. Numerical Fraction (ϕ) of Group Moieties Composing DVB80% PolyHIPE Solid Foams as Determined by ^{13}C CPMAS NMR and Their Solubility Parameter Components

Group	ϕ	δ_{di}^a	δ_{pi}^a	δ_{hi}^a	δ_{a}^a
	0.3	17.2	8.3	7.1	20.4
	0.5	17.8	7.2	8.0	20.8
	0.2	17.4	7.0	7.3	20.1
Poly(DVB80%)	-	17.5	7.5	7.6	20.5

^a For each chemical group the total solubility parameters (δ_{ti}) and their components were calculated according to the method of Hoy.¹⁸

(Figure 10c), which is characterized by a very high surface area, voids of about $1\ \mu\text{m}$ (indicated with a filled circle) appear spherically symmetrical and the diffusion layer across the void boundary is much thinner. This is unequivocally the result of much less intense diffusional fluxes originating from smaller droplets. When T is used as the porogen in connection with the mixture of surfactant, no sign of diffusion is discernible around small droplets (Figure 10d). The surface area of X80PV90(1T)S20AD is slightly higher than that of X80PV90(1CB)S20AD and considering that it differs from that of poly(DVB(T)) by about 5% only, it can be concluded that water diffusion is almost completely prevented.

To test the possibility that the temperature of polymerization exerts an influence on the surfactant cmc , the polymerization of several solid foams was carried out at $100\ ^\circ\text{C}$ and the values of their surface areas as determined by nitrogen adsorption were compared with those of solid foams of the same composition but obtained at $60\ ^\circ\text{C}$. Results are reported in Table 4. As can be seen, for both X80PV90(1CB)S80 and X80PV90(1CB)S20AD the values of surface areas obtained either at 60 (Table 2) or $100\ ^\circ\text{C}$ are the same within experimental error. This is not a surprising result considering the chemical structure of the surfactants used in the present study. Usually, a strong dependence of cmc on temperature is expected for those surfactants containing a poly(ethylene oxide) moiety in their structure capable of undergoing chain contraction or expansion (a phenomenon accompanied, in appropriate conditions, by phase inversion) with temperature variation. The surface area of X80PV90(0.5CB+0.5CEB)S20AD seems to exhibit a slight dependence on temperature (compare entry 11 of Table 2 with entry 3 of Table 4). From results obtained for X80PV90(1CB)S20AD, the nature of the primary surfactants can be ruled out as the cause of this small temperature effect. Therefore, it seems more reasonable to ascribe it to the composition of the porogenic mixture and in particular to the presence of

CEB. It is impossible at this stage of the investigation to assess whether this temperature dependence is a consequence of a variation in the interfacial surfactant/cosurfactant structure or reflects the influence of temperature on the partition coefficient of CEB. In any case, the effect of temperature is modest.

The evidence offered by TEM images (Figure 10), which seems to point to a more efficient barrier effect exerted by the mixture of surfactants as compared to SPAN 80 alone, is further supported by measurements of the NMR self-diffusion coefficient of water in the emulsions ($\phi = 0.9$) containing CB as the porogen and either SPAN 80 or the mixture of surfactants (Figure 11). The plots of water diffusion coefficient (D) vs time (hours) are essentially parallel to the time axis. The first point of the plot was recorded 1 h after emulsion preparation, which seems to indicate that the steady state, in which $c(\infty)$ and therefore D are invariant with time (see eq 4 in the preceding paper), is reached within 1 h.

The value of the self-diffusion coefficient of water is found to be $2.7 \times 10^{-10}\ \text{m}^2\ \text{s}^{-1}$ in the presence of the mixture of surfactants and $6.9 \times 10^{-10}\ \text{m}^2\ \text{s}^{-1}$ in the presence of SPAN 80. These results further support the evidence reported so far that the transfer of water out of the dispersed aqueous phase and its diffusion through the continuous phase is hampered more effectively when the mixture of surfactants is employed instead of SPAN 80. The measurement of the water diffusion coefficient was carried out also for emulsions characterized by different fractions, ϕ , of the dispersed phase, that is 0.75, 0.85, and 0.92, for both surfactant systems. Diffusion curves at different ϕ were coincident for both sets of emulsions within experimental error. This implies that, for the emulsions containing either SPAN 80 or the mixture of surfactants and CB as a porogen, no difference in the surfactant excess at the interface should be expected, as the extent of diffusion is the same for all emulsions having different ϕ . The difference in surface areas, which as already pointed out previously depends on the quality of the solvent medium, should then be ascribed to differences in the extent of interaction among droplets of the dispersed phase (the parameter $f(\phi)$ in eq 4, preceding paper). Figure 10a shows that in the case of solid foams characterized by a pore volume of 75%, droplets are on average more separated than in the case of solid foams with higher pore volume (92%, Figure 10b). As a consequence, the superimposition of diffusion spheres is less pronounced and the worsening of the quality of the solvent medium is less marked. As the volume fraction of the dispersed phase increases, water droplets come closer and closer together and their diffusion domains superimpose to a greater extent. As a consequence, the local concentration of water molecules in these areas is higher and the quality of the solvent toward the growing polymeric network worse. In the case of the mixture of surfactants, the barrier effect exerted by the surfactant film toward diffusion is much more effective and the dependence of diffusion on pore volume far less important as indicated by the substantial constancy of surface areas vs pore volume (Table 2).

As has already been pointed out, when C_2B is used as a porogen together with the mixture of surfactants, a solid foam, X80PV90(1 C_2B)S20AD, with the lowest surface area (among solid foams prepared with the mixture of surfactants) is obtained although it is the

Table 4. Nitrogen Adsorption Results for PolyHIPE Solid Foams Obtained at a Polymerization Temperature of 100 °C

sample	surface area (m ² /g) ^a	V _p (cm ³ /g) ^{b,c}	⟨D _w ⟩ (nm) ^{b,c}	micropore vol (cm ³ /g) ^d	micropore area (m ² /g) ^d
X80PV90(1CB)S80	334 ± 25	0.91 ± 0.09	11.0 ± 0.6	0	0
X80PV90(1CB)S20AD	703 ± 24	0.91 ± 0.08	5.1 ± 0.08	0.12 ± 0.009	47 ± 8
X80PV90(0.5CB+0.5CEB)S20AD	693 ± 31	0.88 ± 0.05	5.2 ± 0.2	0.005 ± 0.003	26 ± 12

^a From BET treatment of N₂ adsorption data. ^b See text for definition of terms. ^c From BJH treatment of N₂ adsorption data. ^d From *t* plot.

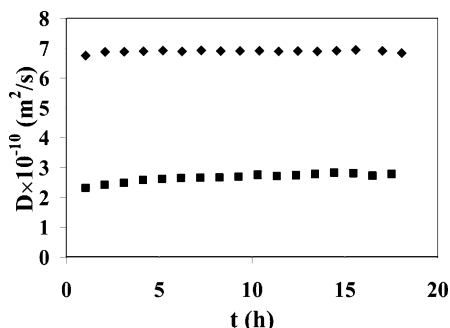


Figure 11. Self-diffusion coefficient of water, at 25 °C, in two emulsions of the same composition of the continuous and dispersed phases (DVB 80% and CB) but incorporating two different surfactants: (◆) SPAN 80; (■) mixture of SPAN 20, DDBSS, and CTAB.

best porogenic solvent for DVB 80%.⁸ Conversely, when C₂B is used together with SPAN 80 the solid foam produced has the highest surface area among S80 type solid foams.⁸ The sets of data presented in this and the preceding paper indicate that the interaction between surfactants and porogens is a major factor in determining the final solid foam characteristics. In particular, we believe that in such interactions, a fundamental role is played by the intrinsic physical properties of the porogens, that is polarity and hydrogen bonding capabilities. When surface area data¹ of solid foams of the X80PV90(1Por)S80 type are arranged according to porogen polarity, a maximum is reached at C₂B which is characterized by a value of δ_p and δ_h midway between those of CB and CEB.

CB (similar considerations apply for T) has, among the porogens examined here, a relatively low polarity and shows limited interfacial activity. This means that, because its ability to penetrate the surfactant layer is limited, the reduction of the interfacial tension is also relatively low. At the same time, it is a sufficiently polar molecule to confer to the organic phase the capability of dissolving a relatively large amount of water. This balance is clearly shifted toward the latter contribution because, as shown by N₂ adsorption data (preceding paper, Table 2, entry 2), the organic medium in the precursor emulsion is a relatively poor solvent thermodynamically for poly(DVB 80%).

At the other end of the polarity scale there are CEB and CPP, which as has been shown previously, exhibit a good ability to penetrate the surfactant monolayer and (presumably) reduce the interfacial tension. At the same time, their values of δ_p and δ_h are high enough so that the equilibrium concentration of water dissolved in the organic phase ($c(\infty)$) and its aqueous/organic phase partition coefficient are the highest. The action of CEB molecules adsorbed at the interface seems to be only to lower the interfacial tension and not to contribute to the formation of a physical barrier against the transfer of molecules through the interface. The difference in values of surface areas between DVB(CEB) (800 m² g⁻¹)

and X80PV90(1CEB)S80 (430 m² g⁻¹) is relevant and can only be explained by assuming that diffusion and partitioning of CEB molecules are still taking place extensively.

C₂B is a molecule which, in terms of polarity and hydrogen bond capability, is midway between CB and CEB. Its behavior resembles closely that of the mixture of CB and CEB. The morphology of the solid foam obtained by employing C₂B as a porogen is characterized by a partially collapsed structure as evidenced by SEM (preceding paper, Figure 2b) and the TEM micrograph (preceding paper, Figure 3b) shows that the degree of overlapping of voids is higher than in X80PV90(1CB)-S80 but less than those of X80PV90(1CEB/CPP)S80. In other words, the drop in interfacial tension caused by the adsorption of C₂B molecules at the interface is high enough to provoke a substantial thinning of the interfacial layer which is responsible for the partially collapsed structure that characterizes this solid foam.

This may mean that C₂B presents the best compromise between several effects working in opposition to each other:

1. Its tendency to be adsorbed at the interface thus reducing Ostwald ripening through its contribution to lowering the interfacial tension.
2. Its polarity and hydrogen bonding formation capability, on the contrary, promoting both water dissolution in the organic phase and the extent of its partitioning between the two phases.
3. Its influence on surfactant c_{uc} and as a consequence on the degree of covering of the interfacial layer by the surfactant molecules.

We can conclude that when SPAN 80 is used as a surfactant, the structure of the final solid foam is dictated by the physical properties of the porogens employed. When C₂B or the 1:1 mixture of CB and CEB are used, the combined influence of γ and $c(\infty)$ on $\omega(t)$ is at its minimum and the solid foams prepared from such porogens are characterized by the highest surface areas.

When the mixture of surfactants is used, a completely different behavior is observed in connection to the nature of the porogens used. When the surface areas (Table 2) are considered as a function of the values of δ_p and δ_h of the porogens used, no clear trend is discernible. Conversely, when differences between the surface areas of the resins and solid foams prepared with the same porogen are arranged according to the polarity of the porogen employed, it can be seen that, with the exception of C₂B, as the polarity of the porogen increases, the said difference in surface areas increases, indicating that the solvent quality decreases in the same fashion. When the 1:1 mixture of CB and CEB is used, the surface area of the corresponding solid foam is slightly lower than that of X80PV90(1CB)S20AD but significantly higher than X80PV90(1C₂B)S20AD. This effect can again be explained in terms of insertion of polar additive molecules between adjacent surfactant

molecules. Clearly a high polarity of the porogen corresponds to a decreased interaction between the ionic components of the surfactant mixture. This effect was described a long time ago by Winsor²³ and is responsible for the dramatic variation of the cmc of ionic surfactants when present in polar solvents. As a result of this "spacing" between the ionic groups, attractive interactions among headgroups, which are probably responsible for the formation of a compact interfacial film, are subdued and contact between the aqueous and exposed organic phase is enhanced. As a result water and porogen molecules can diffuse through the continuous phase, worsening substantially the quality of the reaction medium. There is no simple explanation for the peculiar behavior exhibited by C₂B, which deviates dramatically from the trend described above. Clearly, the effect of this porogen on the surfactant interfacial layer is somewhat disruptive as evidenced indirectly by the large difference in surface areas between poly(DVB-(C₂B)) and X80PV90(1C₂B)S20AD. A possible explanation may be related to the chemical structure of this molecule which in comparison to the other porogens employed is sterically bulkier and its insertion in the interfacial surfactant layer may break down partially the continuity of the surfactant interfacial film. It was shown that the orientation of substituents on the aromatic ring is important in affecting the geometry of surfactant aggregates and the value of the cmc.²⁴ This is also confirmed by the porosity data relative to X80PV90(0.5CB+0.5CEB)S20AD (Table 2). Although polarity and hydrogen bonding abilities of this mixture of porogens (6.1 and 3.0, respectively) are close to those of C₂B (6.3 and 3.3, respectively) the surface areas of the solid foams prepared with these two porogens are very different. This tends to confirm that the peculiar behavior of C₂B as a porogen when used in conjunction with the mixture of surfactants is due to steric effects.

Conclusions

The effect of oil-soluble porogenic solvents on the morphology and microstructure of PolyHIPE solid foams prepared using a three-component surfactant mixture is described. It is concluded that the mixed surfactant system severely limits the extent of Ostwald ripening in the solid foams for all cases except where 1,2-dichlorobenzene (C₂B) is used as porogen. The result of this is surface area values which are much closer to the "true" values obtained for the polymerization of divinylbenzene in the presence of each solvent under investigation. Evidence for the lack of Ostwald ripening is found in the much reduced variation in surface area as the pore volumes of the solid foams are increased, in contrast to the case where SPAN 80 is used as surfactant. Further evidence is provided by NMR experiments of the self-diffusion of water when SPAN 80 and the mixed surfactant system are employed, the results of which indicate that diffusion in the latter case is much lower. The peculiar case of C₂B is rationalized by the suggestion that its adsorption at the interface causes a marked disruption of the packing of surfactant molecules due to its 1,2-disubstituted aromatic structure.

This allows greater migration of water molecules from the aqueous into the organic phase, thus lowering the solvent quality of the latter and leading to lower surface areas.

Acknowledgment. The authors thank the EPSRC for funding this research (GR/M02194) and Dr. D. C. Apperley of the EPSRC solid state NMR national facility at the University of Durham for performing solid state NMR spectroscopy.

References and Notes

- (1) Barbetta, A.; Cameron, N. R. *Macromolecules* **2004**, *37*, 3188.
- (2) Hainey, P.; Huxham, I. M.; Rowatt, B.; Sherrington, D. C.; Tetley, L. *Macromolecules* **1991**, *24*, 117–121.
- (3) Tadros, T. F.; Vincent, B. In *Encyclopedia of Emulsion Technology*; Becher, P., Ed.; Marcel Dekker: New York, 1983; Vol. 1.
- (4) Alexander, A. E.; Schulman, J. H. *Trans. Faraday Soc.* **1940**, *36*, 960–964.
- (5) Barry, B. W. *Rheol. Acta* **1971**, *10*, 96–105.
- (6) Hallworth, G. W.; Carless, J. E. *J. Pharm. Pharmacol.* **1972**, *24*, 71P–83P.
- (7) Bass, R. M.; Brownscombe, T. F. PCT Int. Appl., WO 97/45479, 1997.
- (8) Cameron, N. R.; Barbetta, A. *J. Mater. Chem.* **2000**, *10*, 2466–2472.
- (9) Brunauer, S.; Emmett, P. H.; Teller, E. *J. Am. Chem. Soc.* **1938**, *60*, 309.
- (10) *Porosity and pore size distribution of materials*, BS 7591, Part 2; British Standards Institute: London, 1992.
- (11) Tai, H.; Sergienko, A.; Silverstein, M. S. *Polymer* **2001**, *42*, 4473–4482.
- (12) Sing, K. S. W.; Everett, D. H.; Haul, R. A. W.; Moscou, L.; Pierotti, R. A.; Rouquerol, J.; Siemieniewska, T. *Pure Appl. Chem.* **1985**, *57*, 603–619.
- (13) Webb, P.; Orr, C. *Analytical Methods in Fine Particle Technology*; Micromeritics Instrument Corp.: Norcross, GA, 1997.
- (14) Goldberg, A. H.; Higuchi, W. I. *J. Pharm. Sci.* **1969**, *58*, 1341–1352. Yotsuyanagi, T.; Higuchi, W. I.; Ghanem, A. H. *J. Pharm. Sci.* **1973**, *62*, 40–43.
- (15) Kabal'nov, A. S.; Shchukin, E. D. *Adv. Colloid Interface Sci.* **1992**, *38*, 69–97.
- (16) Nyhus, A. K.; Hagen, S.; Berge, A. *J. Polym. Sci., Part A: Polym. Chem.* **1999**, *37*, 3973–3990. Nyhus, A. K.; Hagen, S.; Berge, A. *J. Appl. Polym. Sci.* **2000**, *76*, 152–169.
- (17) Albright, R. L. *React. Polym.* **1986**, *4*, 155–174. Okay, O. *Prog. Polym. Sci.* **2000**, *25*, 711–779.
- (18) van Krevelen, D. In *Properties of Polymers*, 3rd ed.; Elsevier: Amsterdam, 1991; Chapter 7, p 189.
- (19) Lifshitz, I. M.; Slezov, V. V. *Phys. Chem. Solids* **1961**, *19*, 35. Wagner, C. Z. *Elektrochem. Angew. Phys. Chem.* **1961**, *65*, 581–591.
- (20) Weers, J. G. In *Modern Aspects of Emulsion Science*; The Royal Society of Chemistry: Cambridge, U.K., 1998; 292–327.
- (21) Brailsford, A. D.; Wynblatt, P. *Acta Metall.* **1979**, *27*, 489–497. Marqusee, J. A.; Ross, J. *J. Chem. Phys.* **1984**, *80*, 539–543. Voorhees, P. W. *J. Stat. Phys.* **1985**, *38*, 231–252. Beenakker, C. W. J. *Phys. Rev. A: Atom. Mol. Opt. Phys.* **1986**, *33*, 4482–4485.
- (22) Enomoto, Y.; Kawasaki, K.; Tokuyama, M. *Acta Metall.* **1987**, *35*, 907–913.
- (23) Winsor, P. A. *Manuf. Chem.* **1956**, *27*, 89–95. Winsor, P. A. *Manuf. Chem.* **1956**, *27*, 130–133.
- (24) Horbaschek, K.; Hoffmann, H.; Thunig, C. *J. Colloid Interface Sci.* **1998**, *206*, 439–456. Buwalda, R. T.; Stuart, M. C. A.; Engberts, J. B. F. N. *Langmuir* **2000**, *16*, 6780–6786.

MA035944Y